Characteristic Analysis of the Response Mechanics of Asymmetric High-rise Buildings Subjected to Transverse Wind Loads Considering Second-order Vibration Patterns

Xin Zuo[1], Die Liu[1,*] and Ze Xu[2]

[1]*Business School, Chongqing University of Humanities and Technology, Hechuan, 401520, Chongqing, China*
[2]*School of Resources and Safety Engineering, Central South University, Changsha, 410075, Hunan, China*
E-mail: liudie111@163.com
[*]*Corresponding Author*

Received 01 September 2023; Accepted 25 September 2023;
Publication 03 November 2023

Abstract

The share of high-rise structures in China is growing as a response to the ordinary human wishes of today, such as high-rise accommodations and high-altitude enjoyment facilities. Because of the different traits of high-rise buildings, it is critical to find out about the load response and mechanical traits of high-rise buildings. In this paper, first of all, from the aerodynamic modeling experimental methods on the basis of three-dimensional wind-induced vibration of high-rise structures, high-rise buildings, the side-strain combination of the proposed simple and calculation formula, the basic characteristics of three-dimensional wind-induced vibration of a systematic

European Journal of Computational Mechanics, Vol. 32_4, 313–340.
doi: 10.13052/ejcm2642-2085.3241

study. The modal pushover evaluation technique is then used to analyze the elasticity and plasticity of the high-rise structure, and it is counseled that the higher-order vibration sample has a vital effect on the seismic resistance of the structure. Finally, a calculation principle of the mechanical response of high-rise construction subjected to transverse wind load thinking about the second-order vibration mode is given, and the outcomes exhibit that the Contribution of the second-order vibration mode to the dynamic displacement in the winding course of high-rise construction is inside 2%. However, the most Contribution to the acceleration response can attain 18%.

Keywords: Mechanical characteristics, high-rise buildings, second-order vibration patterns, three-dimensional wind vibration response.

1 Introduction

With the improvement of the economic system and the growth of science and technology, a massive variety of main engineering buildings have been constructed at domestic and overseas in the previous two decades [1]. In the Lujiazui place of Shanghai alone, there are four constructions of over four hundred meters and greater than ten buildings of over 200 meters that have been constructed and are proposed to be built. Developed international locations have even proposed the idea of "sky cities" of the order of 1,000 meters in height. The wind load and response of the shape underneath robust wind is one of the controlling hundreds for the security and serviceability of the shape.

Since 2005, China has defined residential buildings exceeding 10 floors and other civil buildings exceeding 24 meters in height as high-rise buildings. In 1972, the International Conference on Tall Buildings divided high-rise buildings into four categories: the first category is 9 to 16 floors (up to 50 meters), the second category is 17 to 25 floors (up to 75 meters), the third category is 26 to 40 floors (up to 100 meters), and the fourth category is more than 40 floors (higher than 100 meters).

In learning about the wind resistance of high-rise structures, the wind-induced masses are generally divided into downwind loads, crosswind masses, and torsional loads [2, 3]. The downwind load is often composed of the standard wind stress triggered with the aid of the common wind pace and the pulsating wind stress prompted by the incoming pulsation. Since the formation mechanism of downwind wind load is quite simple,

and the equal static wind load generated is incredibly large, it has been paid interest to earlier, and considering that 1960s, Davenport has developed and perfected the calculation technique of downwind wind load and wind response of the structure. The gust wind element approach has been developed [4].

The mechanism of the cross-wind load is very complicated, and it is commonly divided into three types: wake excitation, incoming turbulence excitation, and structural cross-wind action excitation. So far, an entire theoretical technique for the calculation of cross-wind load and its response has no longer been developed. The take a look at outcomes exhibit that beneath identical conditions, the cross-wind pulsation load and its response are generally large than those in the downwind direction, and cross-wind vibration is one of the manipulated elements for the alleviation plan of high-rise buildings [5, 6]. Especially in latest decades, the taller the construction is built, the extra bendy it is, the improved the dynamic response is, and the relief trouble is turning into extra and greater prominent, so the find out about of cross-wind wind load and its response turns into more significant and greater essential.

The torsional wind load is due to the asymmetry of wind stress distribution on the windward side, leeward aspect, and lateral side, which is associated with the turbulence of wind and the vortex in the tail drift of the building. In fact, the human physique is greater touchy to torsional movement than lateral motion, and the torsional response at the area of the construction is especially significant. In general, torsional and lateral vibrations are interrelated and mutually decide the dynamic response of high-rise buildings, and my lateral horizontal vibration is now insufficient to consider the remedy of high-rise buildings, which regularly underestimates the genuine response measurement [7, 8].

The methods of wind resistance research are (1) theoretical analysis method based on random vibration theory; (2) field measurement; (3) experimental study in boundary layer wind tunnel; (4) numerical calculation method based on fluid dynamics – computational wind engineering. In terms of wind resistance research of high-rise buildings, computational wind engineering cannot provide meaningful results yet, while on-site measurements are time-consuming and costly, not very controllable, and not many effective results are available. Therefore, the wind impact lookup of high-rise constructions is typically primarily based on theoretical evaluation strategies and boundary layer wind tunnel experiments.

2 Research on Wind Vibration of Bending and Torsion Coupling of High-rise Buildings

2.1 Several Structural Systems

Several structural systems involved in the paper are explained in advance. Figure 1 shows the non-eccentric high-rise structure, and Figure 2 shows the eccentric high-rise structure; the difference between them only lies in the location of the center of rigidity (referred to as the rigid center), and the center of mass (referred to as the center of mass), other structural parameters are exactly the same [9, 10]. By using a certain order of vibration type Ψ_{xj}, Ψ_{yj}, and $\Psi_{\theta j}$) of the non-eccentric structure, the degrees of freedom of the eccentric high-level structure can be reduced [11].

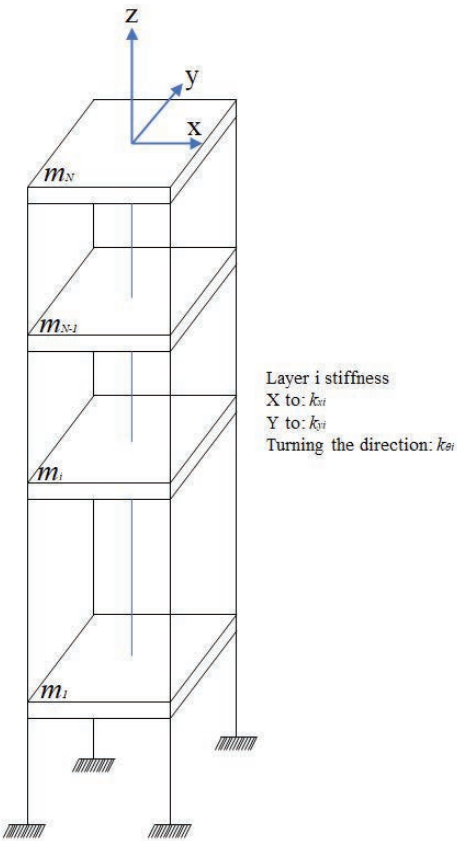

Figure 1 Schematic diagram of an eccentric-free high-level structure.

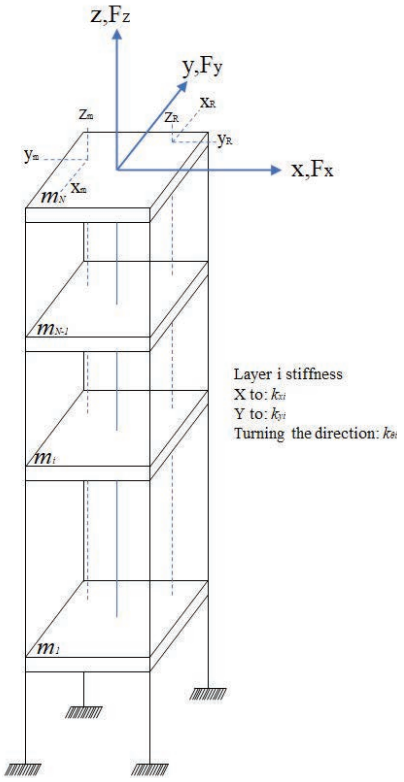

Figure 2 Schematic diagram of the high-level eccentric structure.

2.2 High-rise Eccentric Structure

In this paper, first of all, from the aerodynamic modeling experimental methods on the basis of three-dimensional wind-induced vibration of high-rise structures, high-rise buildings, the side-strain combination of the proposed simple and calculation formula, the basic characteristics of three-dimensional wind-induced vibration of a systematic study.

Without loss of generality, the middle of mass and inflexible core axis of the bending-torsion coupled high-rise constructing are taken to be deviated from the main axis (shape-center axis) at the identical time. The stiffness and mass of the contributors coalesced towards the fundamental axis. The got stiffness matrix and mass matrix are non-diagonal array. The undamped equation of movement of the N-story high-rise construction is (damping will be regarded in the shape of modal damping ratio in the wind vibration

response calculation).

$$[\mathbf{M}]\{\ddot{\mathbf{d}}\} + [\mathbf{K}]\{\mathbf{d}\} = \{\mathbf{F}\} \tag{1}$$

Where M is the overall mass matrix.

$$\mathbf{M} = \begin{bmatrix} \hat{\mathbf{M}}_x & \mathbf{0} & \hat{\mathbf{M}}_{\theta x} \\ \mathbf{0} & \hat{\mathbf{M}}_y & \hat{\mathbf{M}}_{\theta y} \\ \hat{\mathbf{M}}_{x\theta}^{\tau} & \hat{\mathbf{M}}_{y\theta}^{r} & \hat{\mathbf{M}}_{\theta} \end{bmatrix} \tag{2}$$

The diagonal terms of the mass matrix are:

$$\hat{\mathbf{M}}_x = \hat{\mathbf{M}}_y = \hat{\mathbf{M}} = \begin{bmatrix} m_1 & & & \\ & m_2 & & \\ & & \cdots & \\ & & & m_N \end{bmatrix},\ \hat{\mathbf{M}}_\theta = \hat{\mathbf{M}} \times \mathrm{Diag}(\gamma^2) \tag{3}$$

The cross terms of the mass matrix are generated due to the deviation of the center of mass:

$$\hat{\mathbf{M}}_{\mathrm{x}\theta} = \hat{\mathbf{M}}_{\theta x} = -\hat{\mathbf{M}} \times \mathrm{Diag}(\mathbf{y}_{\mathrm{M}}), \hat{\mathbf{M}}_{\mathrm{y}\theta} = \hat{\mathbf{M}}_{\theta y} = \hat{\mathbf{M}} \times \mathrm{Diag}(\mathbf{x}_{\dot{\mathbf{M}}}) \tag{4}$$

Where $\mathrm{Diag}()$ is a diagonal square operator, the result of which is a square matrix with the number of dimensions equal to the number of elements of the vector in the brackets, the diagonal factors of the rectangular matrix are equal to the vector factors, and the non-diagonal elements are 0; $\boldsymbol{\gamma}$ is the radius of gyration vector, defined as the sum of the products of the masses of the masses in the layer and the squared distances from the masses to the vertical axis, and the ratio of the total masses of the layer with an open root, $\boldsymbol{\gamma} = [\gamma_1 \quad \gamma_2 \quad \cdots \quad \gamma_N]$.

K is the overall stiffness matrix, and its submatrix is expressed as follows:

$$\hat{\mathbf{K}}_{ss} = \begin{bmatrix} k_{s1} + k_{s2} & -k_{s2} & 0 & \cdots & & 0 \\ -k_{s2} & k_{s2} + k_{s3} & -k_{s3} & 0 & \cdots & 0 \\ 0 & & & & & \\ & & & & & \\ \vdots & & & & & \\ 0 & & & & & k_{sN} \end{bmatrix},\ s = x, y, \theta \tag{5}$$

Where k_{si} denotes the stiffness in the s-direction of the ith layer, the cross terms $\hat{\mathbf{K}}_{\theta x}$, $\hat{\mathbf{K}}_{x\theta}$ and $\hat{\mathbf{K}}_{\theta y}$, $\hat{\mathbf{K}}_{y\theta}$ of the overall stiffness matrix are generated due to the deviation of the stiff center from the form center axis, and the non-zero elements in the matrix are related to the stiff center coordinates x_{Ri} and y_{Ri} (i = 1,2,...,N).

d denotes the displacement response vector for the longitudinal principal axis position [12, 13].

$$\mathbf{d} = \begin{bmatrix} \mathbf{u} & \mathbf{v} & \boldsymbol{\theta} \end{bmatrix}^T \tag{6}$$

Where *u* is the displacement response vector in the x-direction, $\mathbf{u} = \begin{bmatrix} u_1 & u_2 & \cdots & u_N \end{bmatrix}^T$; *v* is the displacement response vector in the y-direction, $\mathbf{v} = \begin{bmatrix} v_1 & v_2 & \cdots & v_N \end{bmatrix}^T$, and θ is the displacement response vector in the torsion direction, $\boldsymbol{\theta} = \begin{bmatrix} \theta_1 & \theta_2 & \cdots & \theta_N \end{bmatrix}^T$.

The above therapy of mass and stiffness simplifies the equations of motion of the eccentric structure so that the equations can be rewritten as:

$$\begin{bmatrix} \hat{\mathbf{M}} & \mathbf{0} & -\hat{\mathbf{M}}y_M \\ \mathbf{0} & \hat{\mathbf{M}} & \hat{\mathbf{M}}x_M \\ -\hat{\mathbf{M}}^T y_M & \hat{\mathbf{M}}^T x_M & \hat{\mathbf{M}}\gamma^2 \end{bmatrix} \begin{Bmatrix} \ddot{\mathbf{u}} \\ \ddot{\mathbf{v}} \\ \ddot{\boldsymbol{\theta}} \end{Bmatrix} + \begin{bmatrix} \hat{\mathbf{K}}_x & \mathbf{0} & -\hat{\mathbf{K}}_x y_R \\ \mathbf{0} & \hat{\mathbf{K}}_y & \hat{\mathbf{K}}_y x_R \\ -\hat{\mathbf{K}}_x^T y_R & \hat{\mathbf{K}}_y^T x_R & \hat{\mathbf{K}}_\theta \end{bmatrix} \begin{Bmatrix} \mathbf{u} \\ \mathbf{v} \\ \boldsymbol{\theta} \end{Bmatrix} = \begin{Bmatrix} \mathbf{F_x} \\ \mathbf{F_y} \\ \mathbf{F}_{\boldsymbol{\theta}} \end{Bmatrix} \tag{7}$$

Equation (7) represents the form of the structure shown in Figure 2. In this case, the center of mass coordinates x_M, y_M, the radius of gyration γ, and rigid center coordinates x_R, y_R do not vary with height. This paper mainly focuses on this structural system.

2.3 Relationship Between Eccentric High-rise Structure and Single-story Eccentric Structure

2.3.1 Relationship of the basic parameters of the equations of motion

Comparing Equations (1) and (2), the basic parameters of the single-story structure can be determined.

(1) The mass of the single-layer structure is 1, and the radius of gyration is γ.

(2) The stiffness of the single-layer structure in the three major axis directions: $\tilde{k}_{xj} = \omega_{xj}^2 \tilde{m}, \tilde{k}_{yj} = \omega_{yj}^2 \tilde{m}, \tilde{k}_{\theta j} = \omega_{\theta j}^2 \tilde{m} \gamma^2$.
(3) Coordinates of the stiffness center of the single-layer structure: $-\tilde{y}_{Rj} = \frac{\Psi_{\theta j}^T \hat{\mathbf{K}}_x^T \Psi_{xj} y_R}{\omega_{xj}^2 \tilde{m}}, \tilde{x}_{Rj} = \frac{\boldsymbol{\Psi}_{yj}^T \overline{\mathbf{K}}_y \boldsymbol{\psi}_{\theta j} x_R}{\omega_{yj}^2 \tilde{m}}$;
(4) The center-of-mass coordinates of the monolayer structure: $-\tilde{y}_{Mj} = \frac{\boldsymbol{\Psi}_{\theta j}^T \hat{\mathbf{M}}^T \boldsymbol{\Psi}_{xj} y_M}{\tilde{m}}, \tilde{x}_{Mj} = \frac{\psi_{yj}^T \hat{\mathbf{M}} \psi_{\theta j} x_M}{\tilde{m}}$
(5) Loads acting on single-story structures: $F_{sj}^* = \Psi_{sj}^T \mathbf{F}_s (s = x, y, \theta)$

2.3.2 Relationship between vibration mode and frequency

When the primary parameters meet the relationship given in areas (1) and (2), a single-layer shape is equal to the condensed form of a high-rise eccentric structure. It is apparent that the vibration frequency at this time is equal to the frequency of the high-rise eccentric shape [14].

$$\omega_{nj} = \tilde{\omega}_{nj} \tag{8}$$

The vibration mode has the following relationship:

$$\boldsymbol{\varphi}_{nj} = \begin{Bmatrix} \alpha_{xnj} \boldsymbol{\Psi}_{xj} \\ \alpha_{ynj} \boldsymbol{\Psi}_{yj} \\ \alpha_{\theta nj} \boldsymbol{\psi}_{\theta j} \end{Bmatrix} \tag{9}$$

Among them, $\tilde{\omega}_{nj}$ is the nth order frequency of the jth single-layer structure, $n = 1, 2, 3$; ω_{nj} is the frequency of eccentric high-rise structures; $\boldsymbol{\varphi}_{nj}$ is the vibration mode of eccentric high-rise structures; $\alpha_{snj} (s = x, y, \theta)$. The nth-order vibration mode of a single-layer structure can be calculated as follows:

$$\begin{cases} \dfrac{\alpha_{xnj}}{\alpha_{\theta nj}} = \dfrac{\omega_{xj}^2 \tilde{y}_{Rj} - \tilde{\omega}_{nj}^2 \tilde{y}_{Mj}}{\omega_{xj}^2 - \omega_{nj}^2} \\ \dfrac{\alpha_{ynj}}{\alpha_{\theta nj}} = -\dfrac{\omega_{yj}^2 \tilde{x}_{Rj} - \tilde{\omega}_{nj}^2 \tilde{x}_{Mj}}{\omega_{yj}^2 - \omega_{nj}^2} \end{cases} \quad n = 1, 2, 3 \tag{10}$$

Among ω_{xj} and ω_{yj}, the j-th order natural frequencies in the *x* and *y* directions of high-rise non eccentric structures are determined [15].

2.3.3 Relationship between displacement response

According to the vibration mode relationship given in part 2.3.2, it is effortless to attain the displacement response calculation components for eccentric

high-rise structures:

$$\begin{Bmatrix} \mathbf{u} \\ \mathbf{v} \\ \boldsymbol{\theta} \end{Bmatrix} = \sum_{j=1}^{N} \sum_{n=1}^{3} \boldsymbol{\Psi}_j \mathbf{q}_{nj} = \sum_{j=1}^{N} \sum_{n=1}^{3} \boldsymbol{\Psi}_j \boldsymbol{\alpha}_{nj} r_{nj}(t) \tag{11}$$

Among them, $\boldsymbol{\alpha}_{nj} = \begin{Bmatrix} \alpha_{xnj} \\ \alpha_{ynj} \\ \alpha_{\theta nj} \end{Bmatrix}$ is the nth order eigenvector of a single-layer structure; $r_{nj}(t)$ is the nth order generalized coordinate of a single-layer design; $\mathbf{q}_{nj} = \boldsymbol{\alpha}_{nj} r_{nj}(t)$ is the nth order displacement response of a single-layer structure [16].

3 Static Elastic-plastic Analysis Considering the Influence of Higher-order Vibration Modes

The cutting-edge approach for calculating the seismic motion of constructing constructions is the response spectrum technique primarily based on mode decomposition. The use of this algorithm requires the calculation of a couple of herbal vibration intervals and their corresponding modes of the structure, which requires a giant quantity of computation when calculating excessive modes and their corresponding periods, making it tough to manually calculate [17, 18]. Therefore, when conducting structural seismic analysis, the proper response of the shape beneath earthquake motion is regularly approximated through the traits of the shape underneath the fundamental mode of vibration. When the peak of the construction is now not greater than 40 m, the shape is dominated with the aid of shear deformation, and the stiffness and mass are evenly disbursed alongside the height; its seismic motion can be calculated via the backside shear method. This capability is that in seismic design, the above buildings do now not want to think about the impact of excessive modes of vibration and expect that the first mode of vibration is a straight line. This technique is a highly easy approximate calculation method. However, due to the long-standing addiction to examining the seismic response of buildings with the use of the first mode of vibration, it is hard for human beings to precisely replicate the real scenario of the structure in the layout notion of high-rise constructions with the growing wide variety of high-rise and awesome high-rise buildings [19]. Therefore, it is vital to support the evaluation of the impact of excessive mode of vibration on the seismic motion of the shape.

3.1 Modal Pushover Analysis

Pushover is based on the vibrational-type decomposition reaction spectroscopy method, which first disperses the structure into multi-induced systems of multiple particles, and then decomposes the vibrational type of the structure by equating each coefficient of the vibrational type to the corresponding carbonaceous star cluster one-word induced system. Later fiber plasticity analysis method for each equivalent bullet calcination only obtains the free system analysis pushover curve pushover curve into a bilinear equivalence put away, is according to the general equivalence principle of the degrees of freedom system is converted to the base jianli top displacement relationship and the curve should be more district decoupling reaction equation structural force, finally, with SRSS law under each step vibrational type of the structural responses are combined to obtain the response of the whole structure.

3.1.1 Basic assumptions for modal pushover analysis

The basic idea of the modal pushover analysis method is derived from the modal Chemical decomposition spectrum analysis method of the elastic systems. Like ordinary pushover, it still keeps the lateral force or displacement distribution unchanged, but it has better accuracy due to considering multiple modes. The basic assumptions of the modal pushover method are: (1) ignoring the coupling between the various modal coordinates after yielding of the structure; (2) The total seismic demand value of the structure is obtained by combining the sum of squares and square root of each modal response (SRSS).

3.2 Principle of Modal Pushover Analysis

The dynamic equation of a multi diploma of freedom elastic-plastic shape beneath earthquake floor action is:

$$M\ddot{\imath} + C\ddot{u} + f_s(U, \mathrm{sign}\dot{l}) = -\Lambda L\ddot{u}_g(t) \tag{12}$$

M, C represents the system mass and characteristic damping, respectively; *L* is the Unit vector; $f_s = f_s(U, \mathrm{sign}\dot{U})$ restoring force model related to the displacement time history of the structure.

The standard way to solve this coupled equation is through precise RHA [22]. Although modal analysis is unreliable for elastic-plastic systems, we believe that when the amplitude is small, the stiffness of the elastic machine and the preliminary stiffness of the elastic-plastic gadget are the

same, and the two structures have the equal mass and impedance ratio, the vibration traits of the elastic-plastic structural gadget are equal to linear elastic structures with the identical herbal vibration length and mode. The assumption of linear elasticity still applies. The displacement equation of the elastic-plastic system is obtained by extending the displacement equation of the linear elastic system corresponding to the natural vibration mode:

$$\ddot{q}_n + 2\dot{\zeta}_n\omega_n\dot{q}_n + \frac{F_{s'}}{M_n} = -\Gamma_n\ddot{\imath}_{\mathrm{g}}(t) \tag{13}$$

Where $F_{s\nu} = F_{s''}(q, \mathrm{sign}\dot{q}) = \Phi_n^T f_s(U, \mathrm{sign}\dot{l})$, which shows that the lateral forces and the $q_n(t)$ of each order of vibration are related.

Neglecting the coupling effect of each order of vibration, this approximate treatment is one of the foundations of the Chopra modal pushover analysis method. Although all the modes have an influence on the solution of the equation, the Contribution of the nth-order mode is dominant since $q_n(t) = 0$ for all modes in the linear regime, and the coupling between the modes of each order can be ignored [23].

The distribution of the inertial and effective seismic forces for the nth-order vibration pattern is:

$$S_n = \Gamma_n MI\Phi_n \tag{14}$$

$$P_{etfn}(t) = -S_n\ddot{u}_{\mathrm{g}}(t) \tag{15}$$

Here Φ_n corresponds to the vibration type of the linear system, which can be deduced from the equation for the effective seismic force $P_{etfn}(t)$ for the nonlinear system as follows.

$$M\ddot{u} + C\ddot{u} + f_s(U, \mathrm{sign}\dot{U}) = -s_n\ddot{u}_g(t) \tag{16}$$

The solution of the dynamic Equation (16) for the elastoplastic system can no longer be described by the equation $U_n(t) = \Phi_n q_n(t)$ since all vibration modes have an influence on the solution of the equation, but the Contribution of the nth order vibration mode to the structural response is still dominant when analyzing the nth order vibration mode [24]. Accordingly, we can make the following approximation and consider that the approximate response of the structure under the action of the effective seismic force $P_{etfn}(t)$ can be determined by the equation $U_n(t) = \Gamma_n\Phi_n D_n(t)$, where $D_n(t)$ is determined by the following equation [25].

$$\ddot{D}_n + \overset{\leftarrow}{2''_n}\omega_n\dot{D}_n + \frac{F_{s'}}{L_n} = -\ddot{u}_g(t) \tag{17}$$

Among them,

$$F_{s\nu} = F_{s\nu}(D_n, \text{sign}\dot{D}_n) = \phi_n^T f_s(D_n, \text{sign}\dot{D}_n) \tag{18}$$

Equation (17) can be interpreted as the dynamic equation for an elasto-plastic single-degree-of-freedom system corresponding to the nth-order vibration mode, and the single-degree-of-freedom system has the following properties: (1) small-amplitude vibration characteristics – self-oscillation frequency ω_n and damping ratio η_n – corresponding to the nth-order vibration mode of the linear multi-degree-of-freedom system; (2) the $F_{s\nu}/L_n - D_n$ relationship between the resistance $F_{s\nu}/L_n$ and the vibration mode D_n is determined by Equation (18) is determined.

This gives the reaction force of the structure under the action of the total excitation $P_{etfn}(t)$ as:

$$U(t) = \sum_{n=1}^{N} U_n(t) = \sum_{n=1}^{N} \Gamma_n \Phi_n D_n(t) \tag{19}$$

$$r(t) = \sum_{n=1}^{N} r_n(t) = \sum_{n=1}^{N} r_n^{st} A_n(t) \tag{20}$$

4 Simplified Calculation of Wind Vibration Response of Tall Buildings Considering Second-order Vibration Patterns

Wind-induced response includes windward, crosswind, and torsional response, and can be calculated separately for high-rise buildings with symmetrical and regular structural arrangements. For crosswind and torsional steering, the aerodynamic and wind induced response of the structure are related to the cross-sectional form of the structure [26]. Based on the wind tunnel test methods of aeroelastic model, rigid model pressure measurement, and high-frequency force balance, a calculation method for the transverse and torsional wind-induced response of rectangular cross-section high-rise buildings was established. The structural downwind aerodynamic force is mainly caused by downwind turbulence, and its downwind aerodynamic force is related to wind characteristics and the width of the windward surface of the structure, but not to the form of the structural section. Based on the quasi-steady theory, simplified calculation methods for the windward

vibration response of structures are provided in the current building load codes of various countries [27, 28]. Due to differences in the application of national regulations in geomorphic characteristics and wind speed spectra, the calculated wind induced vibration responses of high-rise buildings vary slightly. The proposal of these simplified methods effectively improves the efficiency of structural wind resistance design. However, most of the evaluation methods for wind induced response currently established only consider the contribution of the first order vibration mode, while neglecting the influence of the higher-order vibration mode. As the height of a building increases, its natural frequency decreases accordingly. The contribution of the second-order mode to the wind induced vibration response of the structure cannot be ignored. A simplified calculation method that only considers the contribution of the first-order mode can lead to unsafe results [29]. Zou Yao et al. utilized the crosswind load spectrum of rectangular high-rise buildings and analyzed the contribution of second-order vibration modes to the crosswind response of rectangular high-rise buildings using the frequency domain method. Based on this, a simplified calculation method for the crosswind response of rectangular high-rise buildings considering second-order vibration modes was derived. Compared to the crosswind load spectrum of typical rectangular cross-section high-rise buildings, the frequency band of the crosswind load spectrum is wider, and the contribution of the second-order vibration mode to the windward vibration response of the structure should be highly valued [30].

4.1 Theory of Downwind Wind Response of High-rise Buildings

4.1.1 Calculation method of downwind wind vibration response of high-rise buildings

According to the quasi-constant theory, the normalized downwind generalized load mutual spectrum density function of the i-th order vibration type and the j-th order vibration type mass can be expressed as:

$$S_{FF_i}(f) = \int_0^H m(z_1)\phi_i^2(z_1)\mathrm{d}z_1 \int_0^H m(z_2)\phi_j^2(z_2)\mathrm{d}z_2 \tag{21}$$

Where: B and H are the width and height of the building, respectively; f is the frequency; z_1 and z_2 are the coordinates of any two points in the direction of the width and height of the building, respectively; $m(z_1)$ and $m(z_2)$ are the mass per unit height at heights z_1 and z_2 respectively.

Neglecting the effect of the cross term, the displacement response spectral density function is obtained from the random vibration theory, i.e.

$$S_y(f,z) = \sum_{i=1}^{n} \phi_i^2(z)|H_i(f)|^2 S_{F_i}(f) \tag{22}$$

Where $S_y(f)$ is the generalized load density function of the ith order vibration, ignoring the cross term, $H_i(f)$ is the frequency response function of the ith order vibration, and $\phi_i^2(z)$ is the function of the ith order vibration of the structure at height *z*.

The root mean square response of the displacement at height z of a high-rise building of equal section is calculated by the following equation:

$$\sigma_y(z) = \left[\int_0^{\infty} S_y(f,z)\mathrm{d}f\right]^{0.5} = \left[\int_0^{\infty} \sum_{i=1}^{n} (\phi_i^2(z)|H_i(f)|^2 S_{F_i}(f)\mathrm{d}f\right]^{0.5} \tag{23}$$

And the root mean square response of the acceleration at height z of a rectangular tall building is calculated by the following equation:

$$\begin{aligned}\sigma_y(z) &= \left[\int_0^{\infty} S_y(f,z)\mathrm{d}f\right]^{0.5} \\ &= \left[\int_0^{\infty} \sum_{i=1}^{n} (2\pi f)^4 \phi_i^2(z)|H_i(f)|^2 S_{F_i}(f)\mathrm{d}f\right]^{0.5}\end{aligned} \tag{24}$$

Where $S_y(f,z)$ is the acceleration spectral density function.

4.1.2 Contribution of the second-order vibration pattern to the downwind wind vibration response

For the analysis, the first-order vibration pattern was obtained by fitting the measured and calculated data for the 20 buildings with the expression.

$$\phi_1(z) = \sin\left[\frac{\pi}{2}\left(\frac{z}{H}\right)^{1.8}\right] \tag{25}$$

For the second-order oscillation, the binomial is obtained by fitting the expression.

$$\phi_2(z) = 5\left(\frac{z}{H}\right)^2 - 4\left(\frac{z}{H}\right) \tag{26}$$

Table 1 Main parameters of the model

Model Number	H	B	D	f_1	$\xi_1 = \xi_2$	ρ_b	w_0	Landforms
Model 1	120	60	30	0.556	0.02	240	0.5	A, C
Model 2	160	40	20	0.506	0.02	240	0.5	A, C
Model 3	216	60	20	0.346	0.02	240	0.5	A, C
Model 4	240	60	40	0.222	0.02	240	0.5	B, D
Model 5	280	50	50	0.189	0.02	240	0.5	B, D
Model 6	300	60	50	0.150	0.02	240	0.5	B, D

According to Equations (23) and (24), the Davenport spectra specified in GB50009-2012 "Code for Structural Loads on Buildings" were used to calculate the response of the top part of the structure for different landforms, different self-oscillation frequency ratios f_2/f_1 (f_1 and f_2 are the first- and second-order frequencies in the downwind direction respectively) and different geometries (Table 1), considering only the first-order vibration mode and the first two orders of vibration mode at the same time [31, 32]. The root-mean-square (RMS) response of wind displacement and acceleration in the downwind direction was calculated for the first and second-order vibration modes. The Contribution of the second-order vibration mode to the downwind wind displacement and acceleration response was analyzed, where δ_1 is the root mean square response of the top of the building when only the first-order vibration mode is considered, and δ_2 is the root mean square response of the top of the building when the first two orders are considered. The calculation results are shown in Figures 3 and 4.

From Figures 3 and 4, it can be seen that:

(1) the Contribution of the second-order mode to the downwind wind response of tall buildings decreases as the downwind self-oscillation frequency ratio f_2/f_1 increases.
(2) The Contribution of the second-order mode to the wind response of tall buildings is mainly related to the height of the building, with the Contribution of the second-order mode increasing as the height increases.
(3) The Contribution of the second-order vibration pattern to the root mean square of the downwind displacement of a tall building is generally less than 2%, and the Contribution to the root mean square of the downwind acceleration of a tall building is generally greater than 10%. The maximum Contribution of 18% can be achieved when the structure has a downwind self-oscillation frequency ratio of $\frac{f_2}{f_1} = 2$.

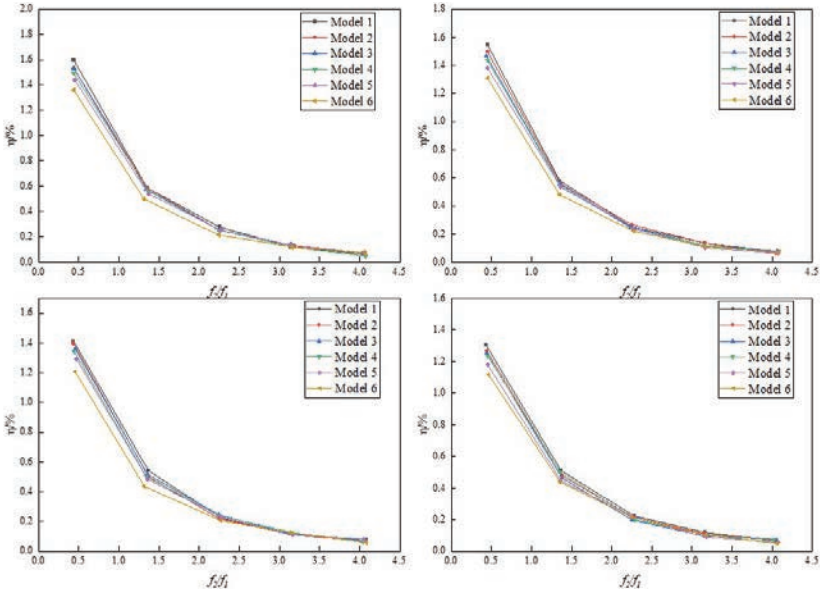

Figure 3 Contribution of second-order vibrational displacement response under different landforms.

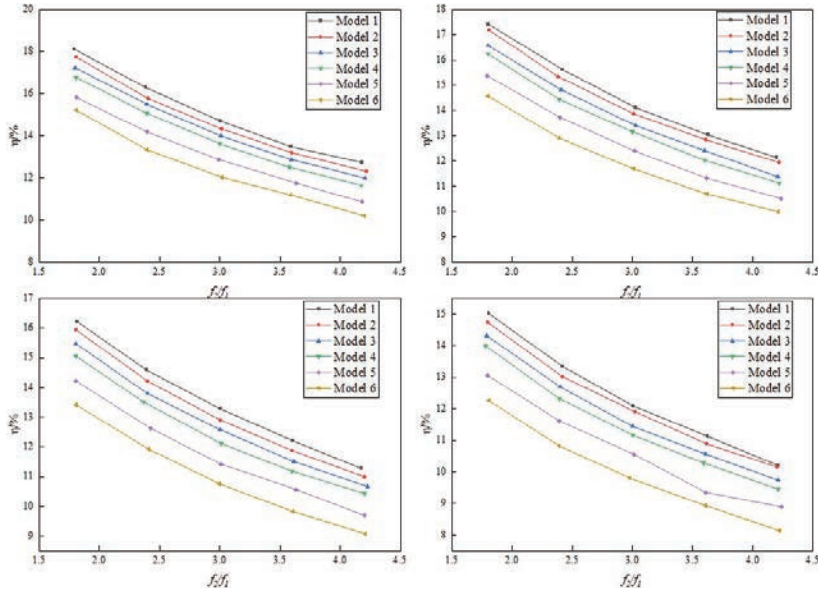

Figure 4 Contribution of second-order vibration to acceleration response under different landforms.

(4) The flatter the terrain, the greater the Contribution of the second-order mode to the root-mean-square response of the building.

4.2 Windward, Crosswind, and Torsional Wind Vibration Displacement Response

The displacement response of a shape in the downwind route is typically giant beneath the motion of pulsating winds, whilst for tall and bendy buildings, the crosswind displacement response is additionally very obvious and, from time to time, even turns into the fundamental influencing factor. The impact of torsional wind displacement response is rather small for high-rise buildings; however, for complicated high-rise structures and adjoining structures with interference, the torsional wind response is different [33, 34]. In this section, the three-d wind vibration displacement response of high-rise constructions is investigated. As the wind load advection-torsion correlation of uncoupled constructions has much less an effect on the displacement response and an extra apparent impact on the acceleration response, this effect is no longer regarded in the following displacement response evaluation.

4.2.1 Influence of structural parameters

Figures 5 and 6 show the variation of displacement response with first-order frequency and damping ratio, respectively (only the first-order vibration type is considered); the torsional displacement of the corner point in the figure is the line displacement generated by the torsion at the corner point *B*. Point *B* is shown in Figure 3. The damping ratio increases from 0.01 to 0.04, and the displacement response decreases from 0.09 m to 0.05 m, a reduction of nearly 1/2. This is because the modal force spectrum has greater energy in the low-frequency region, which also indicates that the factor that has a greater influence on the wind vibration response of the building structure is the first-order self-oscillation frequency. In addition, it can be seen that the cross-wind displacement response is greater than the downwind response.

Since the self-oscillation frequency of a structure is a physical quantity related to the stiffness and mass of the structure, in order to be able to gain insight into the influence of the above parameters on the wind vibration response, the first-order self-oscillation period approximation formula given in the literature [12] is used here, as follows.

$$T_1 = \frac{H\sqrt{\frac{\rho}{P}\frac{1}{R}\frac{\delta}{H}}}{C \times 1.11} \tag{27}$$

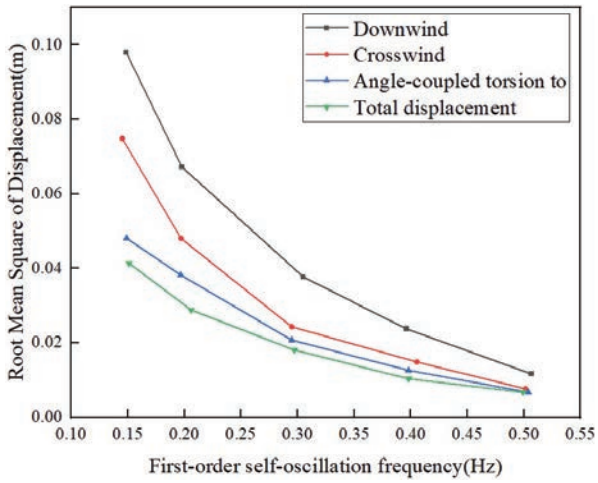

Figure 5 Variation of displacement response with first-order self-oscillation frequency.

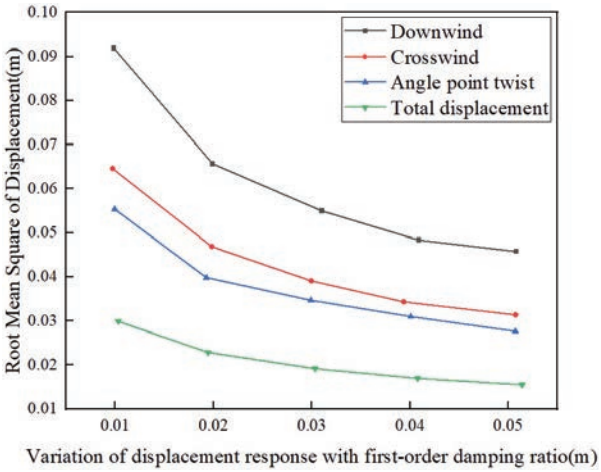

Figure 6 Variation of displacement response with first-order damping ratio.

Where: H is the building height, ρ is the building density, P is the average equivalent wind load, R is the building height-to-width ratio, δ is the standard value of the building top floor excursion, C is the stiffness variation factor along the height, the steel structure is taken as 1.4, the above formula takes into account the density, shape ratio and stiffness of the building, which is more reasonable and convenient in application [35]. Figure 7(a) is the displacement response with the change of building mass density when the

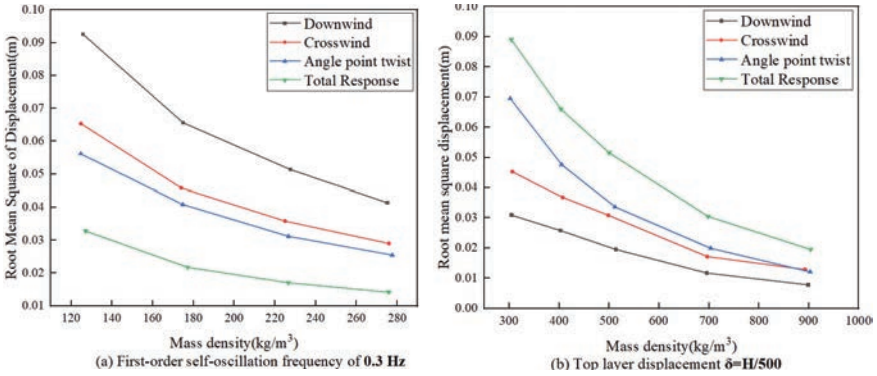

Figure 7 Variation of displacement response with building density.

Table 2 Displacement response in each direction at different lateral shifts

δ	Windward Displacement	Transverse Wind Displacement	Angular Point Torsional Displacement	Total Displacement Response	Horizontal to Total Response Ratio	Torsion to Total Response Ratio
H/300	0.045	0.071	0.028	0.088	63.5%	31.5%
H/400	0.036	0.048	0.024	0.065	54.5%	36.9%
H/500	0.031	0.035	0.022	0.052	45.3%	42.3%
H/700	0.017	0.019	0.016	0.031	37.6%	51.6%
H/900	0.012	0.012	0.014	0.022	29.7%	63.6%

first order self-oscillation frequency is 0.3 Hz, Figure 7(b) is the displacement response with the change of building mass density when the top floor offset 8 = H/500, it can be seen that the displacement response in Figure 7(a) is inversely proportional to the mass density, from the formula (23) know that when the structure self-oscillation frequency is constant, with the increase of structure mass The offset 8 of the top layer of the structure decreases, which increases the lateral stiffness of the structure and the wind vibration displacement response decreases. On the other hand, the increase in mass also reduces the self-oscillation frequency, and the reduction in self-oscillation frequency leads to an increase in response (for the same reason as in Figure 5). As the square of the modal mass is inversely proportional to the modal force, the total displacement response in Figure 7(b) shows a decrease with increasing mass, ranging from 0.061 m to 0.045 m.

Combined with Table 2, it can be seen that the crosswind effect contributes 63.5% to the total displacement response at $\delta = H/300$ and nearly 30% at $\delta = H/900$, a drop of over 30%. The table shows that the

torsional displacement response at corner points does not vary much with stiffness, but relatively speaking, the torsional response contributes more significantly for buildings with greater stiffness, increasing from 31.5% of the total displacement response at $\delta = H/300$ for the lateral shift to 63.6% at $\delta = H/900$.

4.2.2 Influence of Higher-order Modes

In the above analysis, only the first-order mode is considered in each direction, but the higher-order mode also contributes to the total response when the frequencies of the modes are close [38]. The following analysis of the effect of the higher order vibration on the response, for the convenience of the analysis of each direction to take the same higher-order vibration, each direction of the higher order damping ratio of 0.01, the direction of the second and third-order self-oscillation frequency and the first-order self-oscillation frequency in accordance with the ratio of 2.5 to get, the torsion of the higher order to take 2.25 ratio to get, most of the uncoupled high-rise building high-order vibration in line with the law of change. As the frequencies are relatively decentralized, the "square and square" method (SQSS method) can be used to consider the effect of the higher-order vibration pattern on the total response [36, 37]. Figures 8 and 9 show the displacement

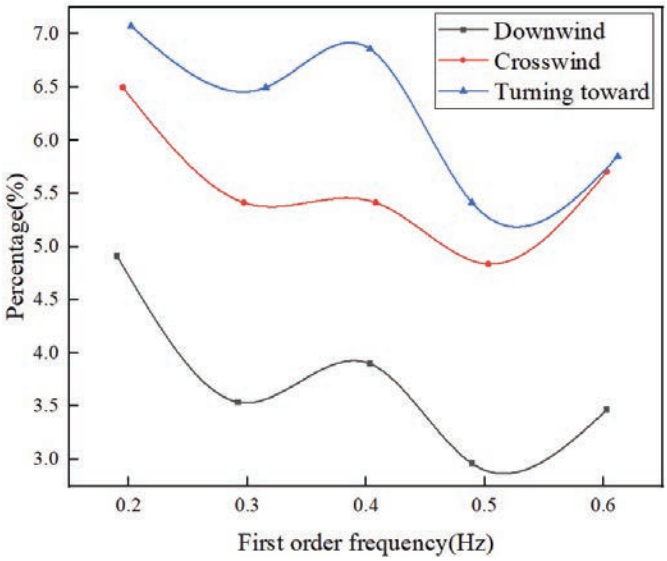

Figure 8 Ratio of second-order response to first-order response.

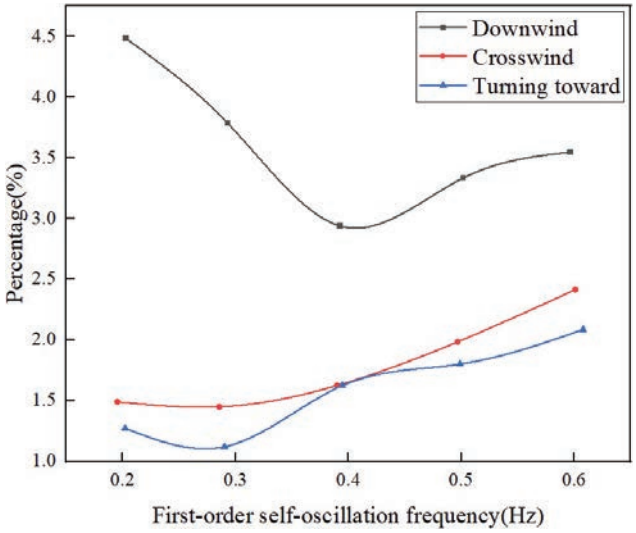

Figure 9 Ratio of third-order response to first-order response.

response of the second and third-order vibration modes at different first-order self-oscillation frequencies compared to the first-order response, with the vertical axis being the percentage of displacement response of the second and third-order vibration modes compared to the first-order response. Figure 8 shows that the second-order displacement response also plays a larger role than the first-order displacement response. The second-order displacement response in the downwind and crosswind directions does not vary much with frequency, accounting for a maximum of about 9% of the first-order response, while the second-order response in the torsion direction is larger, accounting for 18% of the first-order response when the first-order self-oscillation frequency is 0.2 Hz, and decreases to about 9% with the increase of the first-order frequency [39]. The third-order displacement response is relatively small; in different first-order frequencies downwind and crosswind direction, the third-order response accounts for about 2% of the first order, while the maximum torsional third-order response is 4.5%, thus seeing that when considering the effect of higher order vibration on the displacement response, the first two order effects need to be considered for downwind, crosswind and torsional direction, while the third order effect on the response in each direction is smaller in comparison, in order to analyze the torsional displacement response more accurately, the third torsional order response needs to be considered.

5 Conclusion

In this paper, with the intention of organizing an easy and realistic technique for calculating the wind vibration response of high-rise constructing structures, we utilized the random response pushover modal evaluation technique and the time route technique to habits a particular learn about on the static and dynamic wind hundreds as nicely as the wind vibration response of high-rise constructions of complicated physique types, and got here up with some beneficial conclusions, which are typically summarized as follows:

1. Firstly, the motion equation of a torsion coupled high-rise building is given, and the Rayleigh Ritz method is used to simplify the high-rise eccentric structural system into a single-layer structure. Based on this, the influence of stiffness or centroid deviation on the modal of the coupled structure is studied. A calculation method for bending torsional coupled wind induced vibration was derived based on the mode superposition method, and the location of the maximum response at the diagonal point was discussed.
2. This chapter discusses the influence of higher-order vibration modes on the elastoplastic analysis structure of high-rise buildings and also details the modal pushover analysis method based on the vibration mode decomposition response spectrum method, on which some improvements are made. In order to prove the correctness and feasibility of the improvement process, the modal loading function of the commercial software SAP2000 is used to make an example. The results of the example show that the analysis results are very close to the time course analysis when considering the higher order vibration mode on the elastic-plastic phase of the high-rise structure, and the analysis results for the elastic phase of the low-rise and high-rise structures are not yet satisfactory. However, the modal pushover analysis method is still practical for retrofitting and designing seismic-resistant structures.
3. The Contribution of the second-order vibration mode to the downwind wind displacement of the high-rise building is small, but the Contribution to the downwind wind acceleration is large; when the ratio of the second-order to the first-order self-oscillation frequency is 2, the maximum can reach 18%, so when designing the downwind wind acceleration, the Contribution of the second-order vibration mode should be considered. The acceleration response calculated by the integration method considering the second-order vibration mode is greater than the response calculated by the standard method, and only considering the

acceleration response of the first-order vibration mode in the design may not necessarily meet the comfort requirements. Therefore, when designing high-rise buildings, the contribution of second-order vibration modes should be considered.

References

[1] Hou F, Sarkar P P. Aeroelastic model tests to study tall building vibration in boundary-layer and tornado winds[J]. Engineering Structures, 2020, 207: 110259.

[2] Johann F A, Carlos M E N, Ricardo F L S. Wind-induced motion on tall buildings: A comfort criteria overview[J]. Journal of Wind Engineering and Industrial Aerodynamics, 2015, 142: 26–42.

[3] Kim Y C, Bandi E K, Yoshida A, et al. Response characteristics of super-tall buildings–Effects of number of sides and helical angle[J]. Journal of Wind Engineering and Industrial Aerodynamics, 2015, 145: 252–262.

[4] He Wei, Xie Weiping. Research on the fine-grained model of long-span station structure based on comfort evaluation [J]. Journal of Civil Engineering, 2014, 47(1): 13–23.

[5] Zheng Degan, Gu Ming, Zhang Aishe. Numerical simulation of the aeroelastic response of three-dimensional tall building structures based on large eddy simulation [J]. Journal of Building Structures, 2013, 34(9): 97.

[6] Liang S, Zou L, Wang D, et al. Analysis of three-dimensional equivalent static wind loads of symmetric high-rise buildings based on wind tunnel tests[J]. Wind and Structures, 2014, 19(5): 565–583.

[7] Phi L T M, Nguyen T T, Lee J. Buckling analysis of open-section beams with thin-walled functionally graded materials along the contour direction[J]. European Journal of Mechanics-A/Solids, 2021, 88: 104217.

[8] Chan C M, Huang M F, Kwok K C S. Integrated wind load analysis and stiffness optimization of tall buildings with 3D modes[J]. Engineering structures, 2010, 32(5): 1252–1261.

[9] Pan X, Song J, Qu W, et al. An improved derivation and comprehensive understanding of the equivalent static wind loads of high-rise buildings with structural eccentricities[J]. The Structural Design of Tall and Special Buildings, 2022, 31(17): e1976.

[10] Liang S, Liu S, Li Q S, et al. Mathematical model of a crosswind dynamic loads on tall rectangular buildings[J]. Journal of Wind Engineering and Industrial Aerodynamics, 2002, 90(12–15): 1757–1770.
[11] Levin V A, Zubov L M, Zingerman K M. An exact solution to the problem of biaxial loading of a micropolar elastic plate made by joining two prestrained arc-shaped layers under large strains[J]. European Journal of Mechanics-A/Solids, 2021, 88: 104237.
[12] Liang S, Li Q S, Liu S, et al. Torsional dynamic wind loads on rectangular tall buildings[J]. Engineering Structures, 2004, 26(1): 129–137.
[13] Karataº E E, Filippi M, Carrera E. Dynamic analyses of viscoelastic three-dimensional structures with advanced one-dimensional finite elements[J]. European Journal of Mechanics-A/Solids, 2021, 88: 104241.
[14] Kwon D K, Kareem A. Comparative study of major international wind codes and standards for wind effects on tall buildings[J]. Engineering Structures, 2013, 51: 23–35.
[15] Li Shouying, Chen Zhengqing. Study on wind-induced response and equivalent static wind load of super tall buildings [J]. Journal of Building Structures, 2010, 31(03): 32.
[16] Yi J, Zhang J W, Li Q S. Dynamic characteristics and wind-induced responses of a super-tall building during typhoons[J]. Journal of Wind Engineering and Industrial Aerodynamics, 2013, 121: 116–130.
[17] Zheng Yimin, Liu Nanxiang. Calculation of effective range of Stiffness of basement of high-rise structure [J]. Structural Engineer, 2011, 27(4): 17–22.
[18] Nan Z, Kai M, Shaoxue T, et al. Seismic response analysis on isolated connected structure of science museum in Kelamayi[C]//2011 International Conference on Electric Technology and Civil Engineering (ICETCE). IEEE, 2011: 662–667.
[19] Papanikolaou V K, Elnashai A S. Evaluation of conventional and adaptive pushover analysis I: Methodology[J]. Journal of earthquake engineering, 2005, 9(06): 923–941.
[20] Xie L. An improved modal pushover analysis procedure for estimating seismic demands of structures[J]. Earthquake Engineering and Engineering Vibration, 2008, 7: 25–31.
[21] Sasaki K K, Freeman S A, Paret T F. Multimode pushover procedure (MMP) – A method to identify the effects of higher modes in a pushover analysis[C]//Proceedings of the 6th US national conference on earthquake engineering, Seattle, Washington. 1998.

[22] Mahonwang, Lucillin. Some problems in Performance-based seismic design of building structures [J]. Journal of Tongji University: Natural Science Edition, 2002, 30(12): 1429–1434. (in Chinese)
[23] Qu Yue-Qian, Yang Jiang, TANG Wei-Hua. Theory and method of Performance-based seismic design of building structures [J]. Shanxi Architecture, 2009, 35(35): 37–38. (in Chinese)
[24] Moon K S, Connor J J, Fernandez J E. Diagrid structural systems for tall buildings: characteristics and methodology for preliminary design[J]. The structural design of tall and special buildings, 2007, 16(2): 205–230.
[25] Moon K S. Stiffness-based design methodology for steel braced tube structures: A sustainable approach[J]. Engineering Structures, 2010, 32(10): 3163–3170.
[26] Broderick B M, Goggins J M, Elghazouli A Y. Cyclic performance of steel and composite bracing members[J]. Journal of Constructional Steel Research, 2005, 61(4): 493–514.
[27] Faleiro J, Oller S, Barbat A H. Plastic–seismic damage model for reinforced concrete frames[J]. Computers & structures, 2008, 86(7–8): 581–597.
[28] Wu Xue, LI Qiusheng, Li Yi. Surface wind pressure Distribution and wind Load characteristics of complex high-rise buildings [J]. Journal of Building Science and Engineering, 2014, 31(1): 76–82.
[29] Zhao Yunlin. Application Research of Raft Foundation in high-rise building design in Zigong Area [D]., 2010.
[30] Chu Chenhui, Wang Hao. Wind pressure distribution and equivalent wind load of complex tower crown structure of super tall building [J]. Journal of Heilongjiang University of Science and Technology, 2018, 28(4): 471–477. (in Chinese)
[31] Wang Hao, Ke Shitang. Wind-induced response and equivalent static wind load of supertall multi-tower connected buildings based on wind Tunnel Test [J]. Architectural Structures, 2018, 48(21): 103–108.
[32] Song J, Tse K T. Dynamic characteristics of wind-excited linked twin buildings based on a 3-dimensional analytical model[J]. Engineering structures, 2014, 79: 169–181.
[33] Tse K T, Song J. Modal analysis of a linked cantilever flexible building system[J]. Journal of Structural Engineering, 2015, 141(10): 04015008.
[34] Yan B, Li Q S. Wind tunnel study of interference effects between twin super-tall buildings with aerodynamic modifications[J]. Journal of Wind Engineering and Industrial Aerodynamics, 2016, 156: 129–145.

[35] Hu G, Tse K T, Song J, et al. Performance of wind-excited linked building systems considering the link-induced structural coupling[J]. Engineering Structures, 2017, 138: 91–104.
[36] Song J, Tse K T, Tamura Y, et al. Aerodynamics of closely spaced buildings: with application to linked buildings[J]. Journal of Wind Engineering and Industrial Aerodynamics, 2016, 149: 1–16.
[37] Zhu Z, Lei W, Wang Q, et al. Study on wind-induced vibration control of linked high-rise buildings by using TMDI[J]. Journal of Wind Engineering and Industrial Aerodynamics, 2020, 205: 104306.
[38] Holmes J D. Effective static load distributions in wind engineering[J]. Journal of wind engineering and industrial aerodynamics, 2002, 90(2): 91–109.
[39] Park S, Simiu E, Yeo D H. Equivalent static wind loads vs. database-assisted design of tall buildings: An assessment[J]. Engineering Structures, 2019, 186: 553–563.

Biographies

Xin Zuo was born in hechuan, chongqing, P.R. China, in1991, graduated from Chongqing Jiaotong University in 2014 with a bachelor's degree, is now a teacher of Business School of Chongqing University of Humanities and Science and Technology. Her research direction is the intersection of deep neural network and materials.

Die Liu received a master's degree in architecture and civil engineering from Chongqing Jiaotong University in 2016, and began to study for a doctor's degree in civil engineering from Chongqing Jiaotong University in 2022; He is currently a teacher of the Business School of Chongqing University of Humanities and Technology; His research interests include structural health monitoring and big data analysis.

Ze Xu was born in Luoyang, Henan, P.R. China, in1997. He received the Bachelor's degree from Zhengzhou University, P.R. China. Now, he works in School of Civil Engineering, Central South University, P.R. China. His research interests include wind-induced aeroelastic effects and vortex-induced vibration of building structures.